THE ASTROPHYSICAL JOURNAL, 397:260–276, 1992 September 20

OPTICAL SPECTROSCOPY OF Z CANIS MAJORIS, V1057 CYGNI, AND FU ORIONIS: ACCRETION DISKS AND SIGNATURES OF DISK WINDS

ALAN D. WELTY,[1,2,3] STEPHEN E. STROM,[1,3] SUZAN EDWARDS,[3,4] SCOTT J. KENYON,[5] AND LEE W. HARTMANN[3,5]

Received 1992 January 20; accepted 1992 March 23

ABSTRACT

We obtained high-resolution, high signal-to-noise ratio, 3985–4920 Å, 4940–6830 Å, and 8030–9510 Å spectra of V1057 Cyg, Z CMa, and FU Ori at the Mayall telescope at KPNO to examine predictions of the accretion disk model of Kenyon, Hartmann, & Hewett. Synthetic disk spectra are calculated assuming the temperature gradient, $T(R)$, of a classical accretion disk, and assuming that disk photospheres can be modeled by adding contributions from concentric disk annuli represented by spectra of supergiant stars having $T_{\rm eff} \approx T(R)$.

We examine variation of absorption line width with wavelength for synthetic and FUor spectra, and find good correlations for the model and two FUors (V1057 Cyg and Z CMa). We also investigate variation of line width with lower excitation potential and find a subtle effect, less useful as a disk diagnostic.

We subtract synthetic spectra from object spectra to investigate overall goodness of fit. Given the simplicity of the model, we find remarkably good fits for all three objects for wavelengths longer than $\sim$5000 Å. The mismatch at all wavelengths is due to nondisk components to the FUor spectra. We examine these residual features in V1057 Cyg and Z CMa. Most of the strongest features are either emission or P Cygni lines, suggesting origin in powerful winds driven by these objects. For FU Ori, most residuals are absorption features, as expected if FU Ori has lower surface gravity than do supergiants, or if wind absorption is particularly strong.

Subject headings: accretion, accretion disks — stars: individual (Z Canis Majoris, V1057 Cygni, FU Orionis)

1. INTRODUCTION

The FU Orionis objects are pre–main-sequence objects that have experienced large ($\Delta m_{\rm pg} \gtrsim 5$) photometric outbursts, whose rise times vary from as little as 60 days to more than a decade, and which last for decades. Their spectra vary from F or G at optical wavelengths to M in the near-infrared and are characterized by low surface gravity akin to that of supergiants. Large mass-loss rates ($\dot{M} \sim 10^{-5}\ M_\odot\ {\rm yr}^{-1}$) are inferred from H$\alpha$ and Na I D lines, and large infrared excesses are present. More detailed information may be found in articles by Herbig (1977, 1989) and Kenyon & Hartmann (1988), and references therein. Nine such objects are currently recognized: FU Ori (Herbig 1966), V1057 Cyg and V1515 Cyg (Herbig 1977), V1735 Cyg (= Elias 1-12: Elias 1978; Levreault 1983), V346 Nor (= HH 57 IRS 8: Graham & Frogel 1985; Reipurth 1985a), RNO 1B (Staude & Neckel 1991), L1551 IRS 5 (Mundt et al. 1985; Carr, Harvey, & Lester 1987), Z CMa (Hartmann et al. 1989), and BBW 76 (Reipurth 1985b; Eislöffel, Hessman, & Mundt 1990). For the latter three, no outbursts have been recorded, and membership is based on spectroscopic similarity to the former, classical examples.

It is now generally believed that these objects derive their energy from an elevated accretion rate through a circumstellar disk (Hartmann & Kenyon 1985, 1987a, b; Kenyon, Hartmann, & Hewett 1988, hereafter HK1, HK2, HK3, and KHH, respectively). This hypothesis naturally accounts for many of the observed peculiarities in the FU Ori object spectra. A radial temperature gradient accounts for the broad spectral energy distribution (see Lynden-Bell & Pringle 1974, hereafter LBP) and the variation of spectral type with wavelength, since the hot inner region ($T_{\rm max} \sim 7000$ K) dominates in the optical, while the cooler outer regions dominate at longer wavelengths, by virtue of their greater emitting area. Rotation in a disk produces doubled absorption line profiles, as observed in many FU Ori object spectra (e.g., HK1, HK2, HK3). The temperature gradient and differential rotation combine to produce apparent increase in rotational velocity with decreasing wavelength (HK2, HK3) and with increasing lower excitation potential (Welty et al. 1990).

In this contribution, we present high-resolution, high signal-to-noise ratio spectra of Z CMa, V1057 Cyg, and FU Ori covering the 3990–4920 Å, 4940–6815 Å, and 8035–8900 Å ranges. From spectra of supergiant standard stars we synthesize model disk spectra for each object according to the prescription of KHH, for the purpose of making quantitative predictions of the line width versus wavelength and excitation potential relationships, which we then compare to the observed correlations. We subtract the synthetic spectra from the object spectra to determine how well the high-resolution synthetic spectra reproduce observed absorption-line profiles, and whether any real nondisk component to the observed spectra can be inferred from residual features in the difference spectra.

[1] Five College Astronomy Department, The University of Massachusetts, Lederle GRC 517G, Amherst, MA 01003.
[2] Now at Department of Astronomy and Astrophysics, The Pennsylvania State University, 525 Davey Laboratory, University Park, PA 16802.
[3] Visiting Astronomer, Kitt Peak National Observatory, National Optical Astronomy Observatories, which is operated by the Association of Universities for Research in Astronomy, Inc. (AURA), under cooperative agreement with the National Science Foundation.
[4] Five College Astronomy Department, Smith College, Northampton, MA 01063.
[5] Harvard-Smithsonian Center for Astrophysics, Mail Stop 15, 60 Garden Street, Cambridge, MA 01238.

In the disk model context, the cross-correlation results of HK2 and HK3 lead us to expect a steady decrease in line width with wavelength through the optical region. For relatively unblended lines, observed and synthetic spectra of V1057 Cyg and Z CMa reveal the expected effect. For FU Ori, no line width versus wavelength correlation is seen, presumably because its wind perturbs line profiles at short wavelengths (HK2). The uncertainties in the line width versus excitation potential relationship are large, but results for observed and synthesized spectra are consistent for all three objects.

The notion that a wind component may be perturbing line profiles is natural: all FU Ori objects are known, from Hα and Na I D lines, to drive very powerful winds (Bastian & Mundt 1985; Croswell, Hartmann, & Avrett 1987), and postoutburst spectra of FU Ori and V1057 Cyg show blueshifted "shell" features (Herbig 1966, 1977, 1989). Our residual spectra (observed minus synthetic) provide strong evidence that this is the case. We believe this wind component to the metallic line spectrum is particularly strong in FU Ori and obliterates the underlying line width versus wavelength correlation predicted for the disk (cf. HK2, KHH). Further, we believe profiles of residual features will enable us to explore the structure of the outflow, and thus discriminate among competing wind models.

2. OBSERVATIONS AND DATA REDUCTION

We obtained high-resolution, high signal-to-noise ratio spectra of Z Canis Majoris, V1057 Cygni, and FU Orioni, and supergiant standards (required for modeling) with the echelle spectrograph and a charge-coupled device (CCD) detector at the Mayall 4 m telescope at the Kitt Peak National Observatory (KPNO) with integration times of an hour or less per program object. We obtained spectra with wavelength coverage of 3985–4920 Å and 8030–9510 Å on 1988 November 19–21, using KPNO's TI2 CCD. Similar data on the 4949–6830 Å range were obtained on 1988 November 30 using KPNO's TI3 CCD. The TI3 CCD was used for the latter observations because the TI2 CCD was damaged between the two observing runs. In each case, the UV fast camera was employed, with a 31.6 grooves mm^{-1} echelle grating and a 226 grooves mm^{-1} cross-disperser, yielding ~ 11 km s^{-1} resolution at all wavelengths observed. Both TI2 and TI3 are 800 × 800 pixel CCDs, each having 0.015 mm pixels, corresponding to $0''.38$ $pixel^{-1}$ on the sky with our instrument settings.

Each observing night, in addition to object exposures, various calibration images were obtained. Bias frames were taken to correct for the zero integration time CCD response. Flat-field frames (obtained by illuminating the spectrograph and detector system with a "bright quartz" lamp) were obtained to correct for pixel-to-pixel variations in CCD sensitivity. Wavelength calibration was obtained by observing the known spectrum of a thorium-argon hollow cathode before or after each object exposure. A light-emitting diode was used to preflash all exposures to guarantee a background level sufficient to ensure linear CCD response at low light levels.

Data were binned 2:1 perpendicular to the dispersion axis, yielding 800 × 400 pixel echelle images. This was done primarily to save computer tape and disk space and has no significant effect on the resultant spectra. In all cases, the background (sky, scattered solar spectrum) contributes no more than $\sim 5\%$ of the total extracted intensity, except in a number of sharp night sky emission lines (e.g., [O I] and OH lines), and we did not attempt background subtraction. For the 3985–6830 Å data, subtraction of the background is impractical because the narrow decker and $\sim 2''$ seeing left little or no pure background adjacent to the orders. We also wanted to avoid the degradation of signal-to-noise ratio that would be caused by sky subtraction. We did not obtain a 8030–9510 Å spectrum of a rapidly rotating B star, so we are unable to divide out the telluric spectrum, which is significant over much of that region, especially longward of 9000 Å.

The echelle format data were reduced to the final one-dimensional vectors (orders) using the National Optical Astronomy Observatories' Image Reduction and Analysis Facility (IRAF) on the Five College Astronomy Department's Sun386i workstations. The CCD images were debiased and flat-fielded in the usual manner for echelle data. A thorium-argon spectrum obtained after set-up and before observing provides the absolute wavelength calibration for all exposures, and the 0 km s^{-1} reference. The shift between this comparison spectrum and one taken immediately before or after each object exposure, with the telescope pointed at the target, corrects for movement of the CCD detector in its Dewar as a function of telescope orientation. We estimate that errors in our shifts between comparison spectra to be $\lesssim 0.25$ km s^{-1}. Because the count rates are not important for this work, and due to requirements of the program which calculates model disk spectra, all the object spectral orders were normalized to unit continuum.

3. TESTS OF ACCRETION DISK MODEL PREDICTIONS

Hartmann & Kenyon have developed a successful model for the FU Ori objects. We summarize the model and its predictions here; a complete explanation may be found in KHH, and the details of our calculations are given in § 4. An FU Ori outburst occurs when the accretion rate through a circumstellar disk increases, over a period of months to years, and remains at an elevated level for decades after. The accretion luminosity is proportional to the accretion rate (LBP), so the disk brightens. To generate the observed ~ 5 mag increases, the accretion rate must rise by $\gtrsim 2$ orders of magnitude, and we have $L_{\rm disk} \gg L_{\rm star}$. Viscous dissipation near the disk midplane provides internal heating. In the absence of external heating, a temperature gradient perpendicular to the disk midplane is set up by photon diffusion, as in a radiative stellar interior. In the postoutburst state, the central star does not provide significant external heating, so the disk produces its own absorption-line spectrum.

Using the fact that a classical accretion disk also has a radial temperature gradient (LBP), we model the disk spectrum as follows. The disk is divided into many concentric annuli. The spectrum of each annulus is represented by that of a standard star of spectral type appropriate to the "photospheric" temperature of the annulus. These (continuum-normalized) spectra are broadened according to the Keplerian speed of the annuli, weighted according to the relative fluxes expected from annuli of different temperatures, taking geometry and wavelength into account, and summed to produce the final "synthetic disk spectrum." The radial temperature scale of the model is normalized by requiring that the synthesized board-band spectral energy distribution (SED) match the observed SED through the optical and out to ~ 10 μm. Supergiant standards are used for high-resolution spectral synthesis because they provide the best match to observed line strengths.

TABLE 1

LINE WIDTH VERSUS WAVELENGTH RESULTS

Data Set	Slope (km s^{-1} [1000 Å]$^{-1}$)	σ_{slope} (km s^{-1} [1000 Å]$^{-1}$)	Intercept (km s^{-1})	σ_{int} (km s^{-1})	n[a]	r[b]
Z CMa model	−4.20	0.51	113.9	3.4	25	−0.865
Z CMa	−4.30	0.44	116.0	2.9	25	−0.898
V1057 Cyg model	−1.64	0.22	50.6	1.5	65	−0.679
V1057 Cyg	−1.60	0.19	48.5	1.2	65	−0.735
FU Ori model	−2.36	0.43	77.4	2.9	40	−0.665
FU Ori	−0.30	0.30	62.0	2.0	40	−0.156

[a] Number of lines in the data set.
[b] Linear correlation coefficient for the data.

This model makes predictions for potentially observable effects in FU Ori object spectra:

1. Lines formed in a rotating disk should appear doubled, if the disk is viewed at sufficient inclination and spectral resolution (HK1).
2. The hot ($\sim$7000 K) inner disk dominates the optical spectrum, while the larger, cooler outer disk dominates at longer wavelengths; thus the apparent spectral type should be later at progressively longer wavelengths.
3. Line formation should reflect local conditions in the disk. Since the disk is rotating differentially, lines formed in the inner disk (optical lines) ought to be broader, on average, than lines formed in the more slowly rotating outer disk (near-infrared lines).[6]
4. Similarly, lines arising from high excitation potential levels should form preferentially in the inner disk, where temperatures are sufficient to populate those levels.

Thus, we should observe an increase of line width with increasing lower excitation potential. All of these effects have been reported (e.g., Herbig 1977, HK2, HK3, Welty et al. 1990). Here we present a more detailed study of the latter two correlations for our program objects.

We measured widths of individual lines rather than using the cross-correlation technique described in HK1, HK2, and HK3, for the following reasons. Measurement of individual lines permits a more detailed investigation of the line width versus wavelength correlation than does the cross-correlation technique. The search for a line width versus excitation potential correlation is not possible with cross-correlation methods. Further, to investigate the predicted effects, we wish to avoid inclusion of lines that have been strongly affected by nondisk features. Because line width is predicted to vary with both wavelength and excitation potential, we will restrict the range of excitation potential when investigating variation of line width with wavelength and examine the line width versus LEP relationship in restricted wavelength ranges.

Our first step was to identify all the relatively strong ($W_\lambda \gtrsim$ 50 mÅ) absorption lines in our FU Ori object spectra; lines weaker than $\sim$50 mÅ generally cannot be measured with $\lesssim$10% uncertainty, owing to line broadening and finite signal-to-noise ratio of our data. Line identification was accomplished by comparing object spectra with spectra of standard stars, solar spectrum line lists (Swenson et al. 1970; Moore, Minneart, & Houtgast 1966), and the Revised Multiplet Table (Moore 1959). The region around each strong absorption feature was compared with the corresponding line in a standard star of comparable spectral type to remove blended lines from the list. Lines were considered to be significantly blended and removed from further consideration if another feature $\gtrsim$10% as strong lay within the typical absorption profile full width at half-maximum for each object.

High spectral resolution observations reveal that line profiles in FU Ori, V1057 Cyg, and Z CMa are doubled, presumably due to line formation in a rotating circumstellar disk (HK2, HK3, KHH, Hartmann et al. 1989). The doubling is so pronounced in Z CMa that fitting a Gaussian or other simple function is impossible. We should not attempt fitting more complicated functions, since we do not have a priori knowledge of the functional form of the broadening. Therefore, having set the local continuum, visual examination of line profiles to determine half-depth points was the method employed for measuring line widths.

Quantitative predictions of the line width versus wavelength and line width versus excitation potential relationships are made by measuring lines in the synthetic disk spectra. In the following sections, we consider only the "best" synthetic spectrum for each program object, as determined in § 4 below.

3.1. *Line Width versus Wavelength*

The widespread acceptance of the accretion disk model for FU Ori objects is based on its fit to the optical and near-IR energy distributions, and prediction of line width decrease toward longer wavelength observed for FU Ori and V1057 Cyg (HK2, HK3). In this section we present the results of our investigation of the latter effect. The results are summarized in Table 1, and we comment below for each object.

3.1.1. *Z Canis Majoris*

The Z CMa model prediction for the 4000–9000 Å region line width versus wavelength correlation is presented in Figure 1*a*. Due to the large rotational velocity, there are few relatively unblended lines in the spectrum of Z CMa. Therefore, we have included all measured lines, regardless of lower excitation potential. Omission of lines with extreme values of LEP yields only marginally different quantitive results. The slope in Figure 1*a* is -4.20 ± 0.50 km s^{-1} (1000 Å)$^{-1}$, and the intercept is 113.9 ± 3.4 km s^{-1}. The results for line width versus wavelength for Z CMa itself appear in Figure 1*b*. The slope, -4.30 ± 0.44 km s^{-1} (1000 Å)$^{-1}$, and intercept , 116.0 ± 2.9 km s^{-1}, are in excellent agreement with model prediction.

[6] This prediction applies to ensembles of spectral lines in restricted wavelength bins (e.g., echelle orders, hence the cross-correlation method employed by HK2 and HK3), as each line may reach its peak strength at a spectral type (i.e., temperature, and therefore disk radius) whose energy distribution peaks at a wavelength significantly different than that of the line itself. This effect probably is responsible for some of the scatter into our line width vs. wavelength figures below.

In making a case for Z CMa's membership in the FU Ori class, Hartmann et al. (1989) did *not* claim evidence for differential rotation based on their cross-correlation analysis. They showed that the 2.3 μm CO absorption line widths in Z CMa are much narrower than predicted by the accretion disk model (0.2 times the 6200 Å region line widths, compared to the model predicted ratio of $\sim$0.5) and are blueshifted by 25 km s^{-1} from the local interstellar velocity. Those CO observations, and the large infrared excess (see Hartmann et al. 1989, Fig. 9), make it clear that a differentially rotating, flat, thin classical accretion disk is not a complete description of Z CMa. Koresco et al. (1991) have shown that Z CMa has an infrared companion, and that the optical source is well matched by an accretion disk energy distribution. We regard the strong line width versus wavelength correlation for optical region lines, and its agreement with accretion disk model prediction, as compelling evidence for differential rotation in an accretion disk in the Z CMa system.

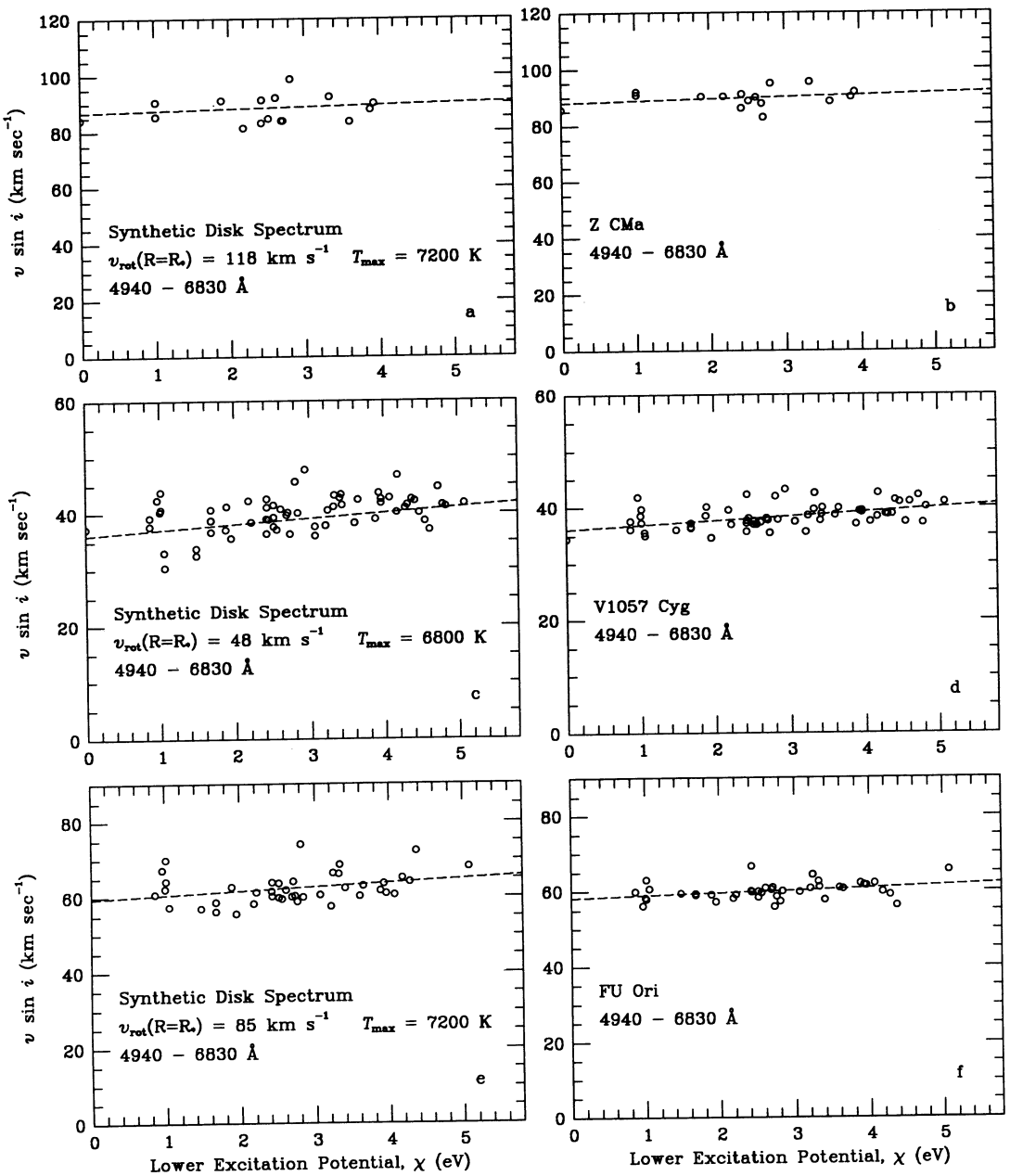

FIG. 1.—We plot line width (interpreted here as rotational velocity $v \sin i$) vs. wavelength for relatively unblended lines in our program objects and corresponding synthetic disk (model) spectra. For Z CMa, the model (*a*) and object (*b*) correlations agree remarkably well. This is the first strong evidence for differential rotation in a Keplerian disk in Z CMa. For V1057 Cyg, the model (*c*) and object (*d*) correlations also agree well, confirming earlier results. For FU Ori, the model (*e*) predicts a correlation that is not seen in the observed spectrum (*f*). This discrepancy has a reasonable explanation that is still consistent with the accretion disk hypothesis (see § 5). We note that high-excitation lines are relatively more common in the far-red region, and low excitation lines are relatively common in the blue. Therefore, we have considered only those lines with $2 \leq 5$ eV for V1057 Cyg and FU Ori to reduce the effect a line width vs. excitation potential correlation would have on this relationship. Because few unblended lines are available for Z CMa, we use them all.

3.1.2. *V1057 Cygni*

The published evidence for variation of line width with wavelength in FU Ori objects, consistent with model prediction, is strongest for V1057 Cyg. Using cross-correlation techniques, Hartmann & Kenyon (HK3) showed that absorption lines in the 6160 Å region are broader than at 2.3 μm, and, unlike their results for FU Ori (JK2, KHH), the synthetic spectrum cross-correlation peak widths agreed well at both wavelengths with those of V1057 Cyg itself. Supporting evidence was provided by Welty et al. (1990), who found evidence for continuous variation of line width with wavelength, but over a shorter wavelength range than the present data provide.

In Figure 1*c* we present the prediction for line width variation as a function of wavelength from the synthetic V1057 Cyg spectrum, spanning the 4000–9000 Å region. Only those lines having $2 < \chi_{low} < 5$ eV have been included so any effect of a line width versus excitation potential correlation on the line width versus wavelength relationship will be reduced. The slope of the least-squares fit to the points is -1.64 ± 0.22 km s^{-1} (1000 Å)$^{-1}$ and the intercept is 50.6 ± 1.5 km s^{-1}, Figure 1*d* is the corresponding graph for V1057 Cyg itself. Points for the same lines as for the synthetic spectrum have been plotted. The slope of -1.60 ± 0.19 km s^{-1} (1000 Å)$^{-1}$ agrees with model prediction well within the uncertainties, although the intercept of 48.5 ± 1.2 km s^{-1} is of marginal agreement. We take this to be strong evidence for differential rotation arising in a circumstellar disk, in the spectrum of V1057 Cyg.

3.1.3. *FU Orionis*

Model prediction of the line width versus wavelength correlation for FU Ori, shown in Figure 1*e*, is much the same as for V1057 Cyg and Z CMa, with exception of the rotational velocity scale. The slope in Figure 1*e* is -2.36 ± 0.43 km s^{-1} (1000 Å)$^{-1}$, and the intercept is 77.4 ± 2.9 km s^{-1}. Results for FU Ori itself, shown in Figure 1*d*, are strikingly different from the model and from V1057 Cyg and Z CMa. There is essentially no slope present. The formal result is -0.30 ± 0.30 km s^{-1} (1000 Å)$^{-1}$ for the slope, and 62.0 ± 2.0 km s^{-1} for the intercept. We offer explanations for this discrepancy from model predictions in § 5.

3.2. *Line Width versus Lower Excitation Potential*

Herbig (1989) described a search for a line width versus LEP correlation in early Lick spectrograms of FU Ori and V1057 Cyg. He found no correlation. He found the same negative result with more recent, higher quality data. This effect was also searched for by Welty et al. (1990), who detected marginal line width versus LEP correlations in 11 km s^{-1} resolution echelle spectra of V1057 Cyg. We have secured multiepoch, high signal-to-noise ratio spectra of broad wavelength coverage, and are able to investigate more completely the question of the existence and repeatability of this correlation.

We have shown that line width decreases significantly over the 4000–9000 Å region in the spectra of V1057 Cyg and Z CMa. To detect a variation of line width with excitation potential, we must restrict the range of wavelength to be considered. We chose to restrict wavelength according to the three observational data sets (3985–4920 Å, 4940–6830 Å, 8030–9000 Å). In the subsections that follow, we present results graphically only for the 4940–6830 Å data. Complete results appear in Table 2.

3.2.1. *Z Canis Majoris*

The 4940–6830 Å line width versus LEP synthetic spectrum prediction is shown in Figure 2*a*. The slope is 0.74 ± 1.16 km s^{-1} eV^{-1}. For Z CMa itself (Fig. 2*b*), the slope is 0.62 ± 0.78 km s^{-1} eV^{-1}. The uncertainties are large primarily because only 16 lines are involved. The close agreement between predicted and observed slopes may be fortuitous.

There are even fewer unblended lines in the blue far-red regions. Results based on them are highly uncertain and do not merit further discussion. We believe firmer results on the existence of a line width versus LEP correlation in Z CMa will be extremely difficult to obtain, because the extensive line blending will remain a serious hindrance.

3.2.2. *V1057 Cygni*

From our best synthetic disk spectrum, the predicted line width versus LEP relationship is shown in Figure 2*c*. The slope of the least-squares fit is 1.13 ± 0.30 km s^{-1} eV^{-1}. We see that, even for the synthetic spectrum, the correlation is not particularly strong. Figure 2*d* shows the observed line width versus

TABLE 2

LINE WIDTH VERSUS EXCITATION POTENTIAL RESULTS

Data Set	Slope (km s^{-1} eV^{-1})	σ_{slope} (km s^{-1} eV^{-1})	Intercept (km s^{-1})	σ_{int} (km s^{-1})	n[a]	r[b]
Z CMa model (λ_2)	0.74	1.16	86.0	3.1	16	0.169
Z CMa (λ_2)	0.62	0.78	88.2	2.1	16	0.208
Z CMa model (λ_3)	0.33	1.41	77.8	3.4	6	0.117
Z CMa (λ_3)	0.63	1.60	77.6	3.9	6	0.193
V1057 Cyg model (λ_1)	0.51	0.88	40.7	2.8	6	0.279
V1057 Cyg (λ_1)	1.23	0.67	38.7	2.1	6	0.679
V1057 Cyg model (λ_2)	1.13	0.30	36.8	0.9	64	0.428
V1057 Cyg (λ_2)	0.77	0.19	36.2	0.6	64	0.452
V1057 Cyg model (λ_3)	0.79	0.27	34.1	1.0	23	0.544
V1057 Cyg (λ_3)	0.82	0.26	33.1	0.9	23	0.569
FU Ori model (λ_2)	1.06	0.58	59.5	1.7	42	0.274
FU Ori (λ_2)	0.64	0.32	58.2	0.9	42	0.302
FU Ori model (λ_3)	2.75	0.69	50.5	1.8	11	0.799
FU Ori (λ_3)	2.13	0.57	53.5	1.5	11	0.778

[a] Number of lines in the data set.
[b] Linear correlation coefficient for the data.

LEP relationship. The slope is 0.77 ± 0.19 km s^{-1} eV^{-1}. So we have agreement of model prediction and observation at the 1 σ level.

In the far-red region (8030–9000 Å), the situation is different. Measurement of the model spectrum yields a slope of 0.79 ± 0.27 km s^{-1} eV^{-1}, and the slope for the V1057 Cyg spectrum is 0.82 ± 0.26 km s^{-1} eV^{-1}. In the blue region (3985–4929 Å), there are too few lines (six) in our list for us to draw any firm conclusions. Complete results for all three wavelength ranges appear in Table 2.

We wish to compare our result with that of Welty et al. (1990), who found similar results with 1986 October and 1986 December spectra of V1057 Cyg. For proper comparison, we must determine slopes for identical line lists. The lists differ due to different gaps in wavelength coverage in the far-red, bad pixels, cosmic-ray hits, etc. For the 36 lines in common in the 5820–6830 Å region, their result would be 0.85 ± 0.24 km s^{-1} eV^{-1}, and ours would be 0.76 ± 0.21 km s^{-1} eV^{-1}. For the 14 lines in common in the 8030–9300 Å region, their result would be 1.23 ± 0.52 km s^{-1} eV^{-1}, and ours would be 1.09 ± 0.45

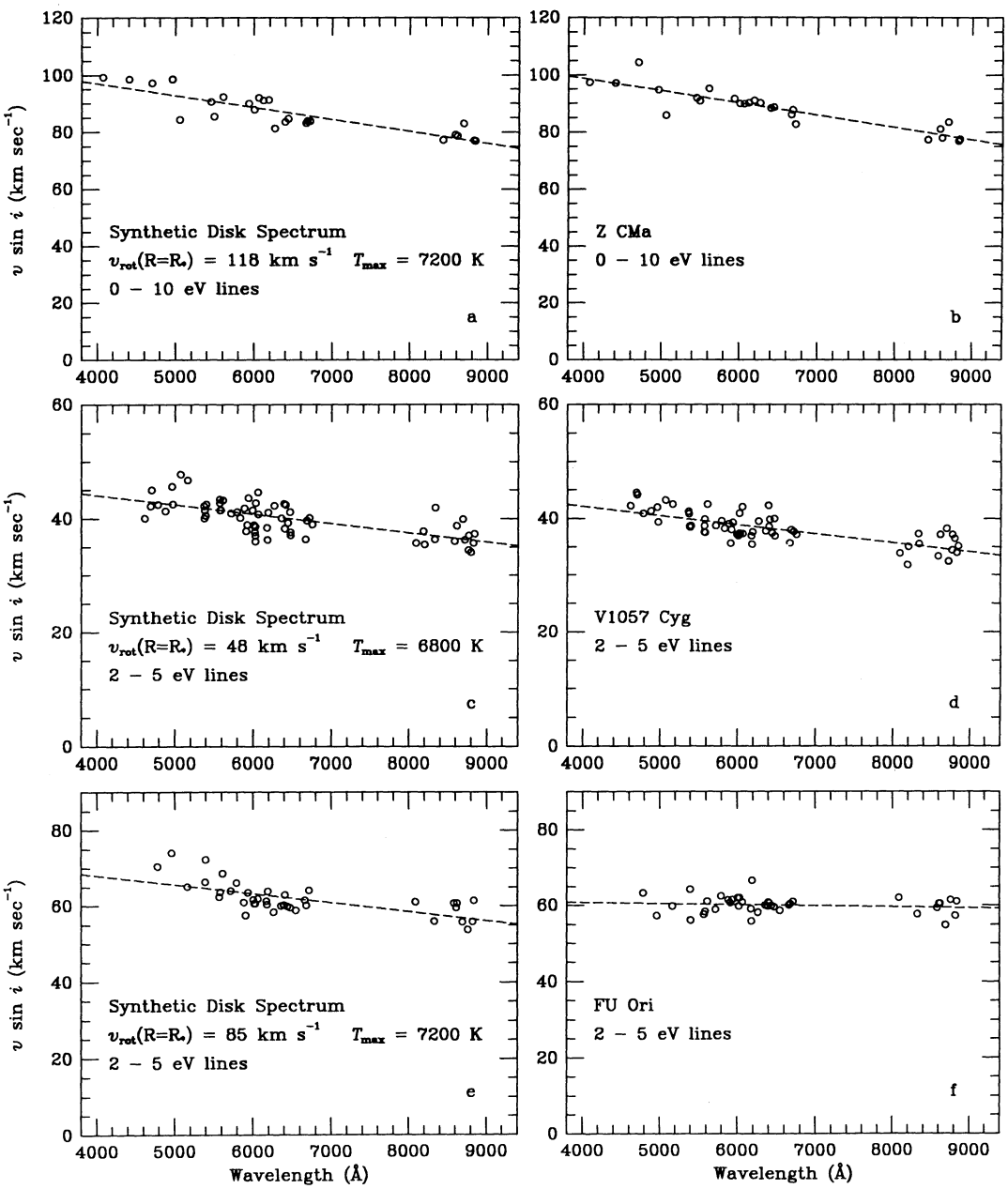

FIG. 2.—Here we plot line width vs. lower excitation potential for unblended lines in our program objects and our best models for them. Only the 4940–6830 Å lines are considered here, to remove some of the scatter that the line width vs. wavelength correlation introduces. The layout is the same as in Fig. 1. The correlations are not strong, but model prediction and observation are consistent (see Table 2). This effect probably is present but is less useful as a diagnostic of differential rotation than the linewidth vs. wavelength relationship.

km s^{-1} eV^{-1}. We take this repeatability as further evidence that a line width versus LEP correlation exists in the spectrum of V1057 Cyg.

3.2.3. *FU Orionis*

In view of our line width versus wavelength results for FU Ori, it would not be unexpected if a line width versus LEP correlation does not exist in the spectrum of this object. The prediction for 4940–6830 Å region, shown in Figure 2*e*, is a slope of 1.06 ± 0.58 km s^{-1} eV^{-1}, and the slope from the FU Ori spectrum is 0.64 ± 0.32 km s^{-1} eV^{-1} (Fig. 2*f*). So it appears that a weak correlation is present, and agreement with the model prediction is good at the 1 σ level.

As is the case for Z CMa, there are too few unblended lines in our blue and far-red spectra to attempt to draw meaningful conclusions from those data. It is interesting, though, that prediction and observation agree, based on 11 points, that a large slope is present in the far-red region. They are, respectively, 2.75 ± 0.69 km s^{-1} eV^{-1} and 2.13 ± 0.57 km s^{-1} eV^{-1}.

In summary, we find evidence for a line width versus excitation potential correlation in the red and far-red spectrum of V1057 Cyg. Similar correlations may be present in Z CMa and FU Ori, but line blending will continue to hamper efforts to make any firm conclusions for these two objects. In any case, the apparent subtlety of the effect, as judged from measurement of synthetic spectra, and the scatter that is present, render this effect less useful as a diagnostic of differential rotation than the line width versus wavelength relationship.

4. SYNTHETIC DISK SPECTRA AND GOODNESS OF FIT

To generate synthetic disk spectra we follow the prescription of KHH, in which we must specify (1) the maximum disk temperature, T_{max}, which occurs at $R = 1.36\ R_\odot$ in a classical accretion disk (LBP); (2) the normalization of the Keplerian rotation curve, expressed herein as $v_{max} = v_{rot}(R = R_*)$; (3) the mapping of standard star spectra to disk annuli; and (4) the relative contribution to the total flux at selected wavelengths from each annulus specified in point (3). The specification of radii, temperatures, and relative weights of disk annuli for our Z CMa and FU Ori models is given in Table 4 of KHH; we used a hotter model for V1057 Cyg than did KHH. Similar "weight tables," calculated for different T_{max}, were used in the analysis described below. The assignments of standard star spectra to the annuli are given in Table 3.

4.1. *Goodness of Fit: Method and Results*

Having generated synthetic disk spectra which sample parameter space near the values suggested by KHH (V1057 Cyg and FU Ori) and Hartmann et al. (1989; Z CMa), we quantify the goodness of fit as follows. We search each object and residual spectrum order (object minus synthetic) for sets of several consecutive pixels that each deviate in the same sense from one or zero, respectively, by more than some threshold value. We define the goodness of fit as $f = 1 - (n_r/n_l)$, where n_r is the total number of pixels in residual features, and n_l is the total number of pixels in absorption lines in the corresponding portion of object spectrum. We define the uncertainty in f as $\sigma_f = (n_r + n_l)^{1/2}/n_l$. The quantity f is essentially the fraction of absorption lines that are well matched by the synthetic profiles. Strong broad features that do not arise in a disk, e.g., the Na I D and Hα wind absorption features, can cause f to be spuriously low. Similar contributions to other lines can drive f to small values, if they are sufficiently numerous. In extreme cases, negative values are possible.

We arbitrarily define a residual feature as one having at least six consecutive pixels deviating at least 0.02 from zero. We use the same value for the threshold for all spectral orders, rather than, for example, some multiple of the rms noise, σ, for each order, so we will not bias the results by requiring stronger (per

TABLE 3

STARS USED FOR HIGH-RESOLUTION SPECTRAL SYNTHESIS

Star Name	Spectral Type	Spectral Range	Line Width (km s^{-1})	Contribution 6800 K	Contribution 7200 K
4000–4920 Å Spectra					
α Lep	F0 Ib	F2–F3	12	...	0.34
α Per	F5 Ib	F4–F7	16	0.53	0.30
μ Per	G0 Ib	F8–G2	13	0.25	0.20
HR 1327	G5 IIb	G3–G5	9	0.07	0.06
ϵ Gem	G8 Ib	K0	12	0.02	0.02
β Gem	K0 IIIb	K1–2900 K	8	0.11	0.08
4940–6820 Å Spectra					
SAO 11104	F0 I	F2–F3	9	...	0.21
SAO 22328	F6 Ib	F4–F8	9	0.43	0.30
SAO 22740	G2 Ib	G0–G5	10	0.24	0.22
SAO 22820	K0 Ib	K0–K1	13	0.06	0.06
SAO 22785	K5 Ib	K2–K5	9	0.14	0.12
SAO 23207	M3 Iab	M1–2100 K	14	0.11	0.10
8030–9300 Å Spectra					
δ Cep	F5 Ib	F2–F7	11	0.23	0.28
β Aqr	G0 Ib	F8–G2	13	0.18	0.16
9 Peg	G5 Ib	G3–G5	12	0.08	0.07
56 Ori	K1.5 IIb	K0–K2	11	0.14	0.13
HR 8726	K5 Ib	K5	12	0.10	0.09
μ Cep	M2 Ia	M1–1300 K	23	0.27	0.26

TABLE 4

GOODNESS OF FIT TEST RESULTS

T_{max} (K)	v_{max} (km s^{-1})	v_{rad} (km s^{-1})	f
Z Canis Majoris			
7065	115	0	0.703
	121	0	0.718
7200	115	0	0.730
	118	0	0.751
	121	0	0.748
	124	0	0.741
	130	0	0.730
7500	115	0	0.716
	118	0	0.734
	121	0	0.748
	127	0	0.738
	130	0	0.733
7660	118	0	0.663
	121	0	0.687
	127	0	0.707
	130	0	0.705
	135	0	0.700
7980	121	0	0.671
	127	0	0.663
7200	118	−8	0.725
	118	−5	0.732
	118	−2	0.747
	118	+2	0.741
	118	+5	0.729
	118	+8	0.707
V1057 Cygni			
6370	48	0	0.798
	51	0	0.795
6590	45	0	0.807
	48	0	0.824
	51	0	0.834
	54	0	0.825
6800	45	0	0.809
	48	0	0.846
	51	0	0.842
	54	0	0.833
	57	0	0.828
6930	45	0	0.815
	48	0	0.838
	51	0	0.840
	54	0	0.833
	57	0	0.828
7065	45	0	0.810
	48	0	0.832
	51	0	0.829
	54	0	0.807
6800	48	−5	0.808
	48	−2	0.829
	48	+2	0.831
	48	+5	0.820
FU Orionis			
6800	80	0	0.788
	85	0	0.801
6930	80	0	0.804
	85	0	0.814
	90	0	0.802
7065	75	0	0.800
	80	0	0.826
	85	0	0.821
	90	0	0.811
7200	70	0	0.796
	75	0	0.818
	80	0	0.827
	85	0	0.829
	90	0	0.806
	95	0	0.786
7500	75	0	0.780
	80	0	0.826
	85	0	0.828
	90	0	0.817
7660	80	0	0.793
	85	0	0.820
	90	0	0.822
	95	0	0.816
	100	0	0.802
7980	85	0	0.743
	90	0	0.747
7200	85	−8	0.798
	85	−5	0.818
	85	+5	0.808
	85	+8	0.785

pixel) residual features in orders having higher noise levels. Even so, results for the relatively low signal-to-noise ratio orders (the first half-dozen or so in the 3985–4920 Å and 4940–6830 Å regions) are less reliable than for high SNR orders. The 0.02 threshold corresponds to a lower limit on equivalent widths of residual features ranging from ~8 mÅ at 4000 Å, to ~17 mÅ at 9000 Å.

The model input parameters that maximize f are assumed to be the correct values and have been used to generate the models discussed in §§ 3 and 5. We calculate f for the portion of the spectrum that appears to be generally well fit (4940–6815 Å for V1057 Cyg and Z CMa, 5900–6815 Å for FU Ori; see below) so poor choices of input parameters will *introduce false residual features*, and not simply alter profiles of real residual features. For each program object, Table 4 show f for a region of input parameter space sufficient to show that the "best" values have been determined. The values for σ_f are 0.011, 0.009, and 0.016 for Z CMa, V1057 Cyg, and FU Ori, respectively. We comment below for each object.

4.1.1. *Z Canis Majoris*

For Z CMa a model with $T_{max} = 7200$ K, $v_{max} = 118$ km s^{-1}, and zero velocity shift with respect to local material maximizes f in the 4940–6815 Å region, with $f = 0.751 \pm 0.011$. $T_{max} =$ 7200 K, and 7500 K models with $v_{max} = 121$ km s^{-1} each yield $f = 0.748 \pm 0.011$. It appears that f decreases more slowly as v_{max} is raised beyond its optimum value than when v_{max} is reduced below that value, for a given T_{max}. We adopt $T_{max} =$ 7350 ± 250 K, and $v_{max} = 120 \pm 5$ km s^{-1}, where the uncertainties correspond to approximate limits of error bar overlap. For this study, no appropriate weight table was available because our supergiant sequence does not include a 7350 K star, and we have used the 7200 K, 118 km s^{-1} model for all subsequent analysis.

For all T_{max}, v_{max} pairs, the radial velocity of Z CMa is constrained to be within ~5 km s^{-1} of the local interstellar gas. In Table 4 we have shown the v_{rad} test results only for the 7200 K, 118 km s^{-1} model; results for other values of these parameters show a similar trend, but with smaller values of f.

4.1.2. *V1057 Cygni*

For V1057 Cyg, a $T_{max} = 6800$ K, $v_{max} = 48$ km s^{-1} model maximizes f at 0.846 ± 0.009 for the 4940–6830 Å region. At these lower temperatures our model temperature grid is finer, and the results in Table 4 suggest that $T_{max} = 6825 \pm 250$ K. The variation of f as function of v_{max} at constant T_{max} is similar to that for Z CMa, and we adopt $v_{max} = 50 \pm 3$ km s^{-1}. We have used a $T_{max} = 6800$ K, $v_{max} = 48$ km s^{-1} model for further analysis because f is maximized for that model. This v_{max} is greater than the KHH value of 43 km s^{-1}. The increase reflects an actual increase of line widths observed in V1057 Cyg spectra spanning the time from their observations until ours.

We find that the radial velocity of V1057 Cyg must be within ~ 2 km s^{-1} of $+15$ km s^{-1}, the radial velocity of neighboring interstellar material. Table 4 shows results of v_{rad} tests only for $T_{max} = 6800$ K and $v_{max} = 48$ km s^{-1}; results for other values of these parameters show a similar trend, but with smaller values of f.

4.1.3. *FU Orionis*

FU Ori's maximum disk temperature also appears reasonably well constrained by our goodness of fit test results, shown in Table 4. We find $T_{max} = 7200 \pm \sim 350$ K, in agreement with the FU Ori temperature scale determined by HK2.

The goodness of fit is maximized for the 7200 K model when $v_{max} = 85$ km s^{-1}. Values as low as 80 km s^{-1} are almost as good. We have used 85 km s^{-1} as the best value because it maximizes f, and our cross-correlation analysis favors it over smaller values.

The FU Ori spectrum synthesis in KHH used $v_{max} = 93$ km s^{-1}. Unlike V1057 Cyg, we have noticed no change in FU Ori's line widths with time. The discrepancy arises because FU Ori's lines are more strongly affected by wind absorption: its lines are somewhat deeper and our goodness of fit algorithm requires narrower and deeper lines to minimize the residuals.

As for our other program objects, the radial velocity of FU Ori is constrained to be within ~ 3 km s^{-1} of the local interstellar gas. Results are given only for tests with $T_{max} = 7200$ K and $v_{max} = 85$ km s^{-1}.

4.2. *Data, Final Models, and Residual Spectra*

Examples of the synthetic disk spectra calculated with the best input values determined above, and corresponding object and residual spectra are presented in Figure 3. Each panel shows, top to bottom, the observed, synthetic, and residual spectrum for Z CMa, V1057 Cyg, and FU Ori, respectively. Among the notable features in Figure 3 are the doubled profiles of many relatively unblended lines, most common longward of ~ 5800 Å, as expected from a rotating disk. Most of the obvious residual features appear in all three program objects.

To quantify the difference in goodness of fit at different wavelengths, we calculated f for 62 wavelength bins, contiguous when possible, each from a single echelle order. Regions of significant telluric contamination have been excluded. We present these results in Figure 4. Several points are lower than their neighbors in one or more objects due to the inclusion of strong broad blueshifted wind absorption features, most notably Hβ, Na I D, and Hα. The 4300 Å region points also have low values of f in part because strong CH features (the G band) make proper continuum normalization of synthetic and object spectra extremely uncertain. Shortward of ~ 5000 Å, the overall fit is not as good because residual features are more common at shorter wavelengths, suggesting origin in a wind. The slight increase in f at the shortest wavelengths is not real: it is an artifact of noise intrusions into features otherwise identifiable by our goodness of fit algorithm.

The synthetic spectra may have fit the observed spectra even better had a more appropriate grid of standards been used. In particular, a finer spectral type grid, spanning the full range required by the model, would be desirable. Nevertheless, our crude models do very well for V1057 Cyg and Z CMa longward of ~ 5000 Å, and for FU Ori longward of ~ 5900 Å.

5. DISCUSSION OF RESIDUAL FEATURES

We have shown that an unmistakable correlation between line width and wavelength exists in high-resolution optical spectra of Z CMa and V1057 Cyg, in excellent agreement with prediction from an accretion disk model which also accounts well for the observed broadband spectral energy distributions of V1057 Cyg and FU Ori (KHH). A correlation between line width and excitation potential, though less obvious, is consistent with model prediction for all three program objects. Those results, the doubled absorption-line profiles, and impressive model fit in the red spectral region all suggest that luminous accretion disks are the dominant contributors to FU Ori object spectra. If true, and if our model disk spectra synthesized from supergiant spectra are good representations of such

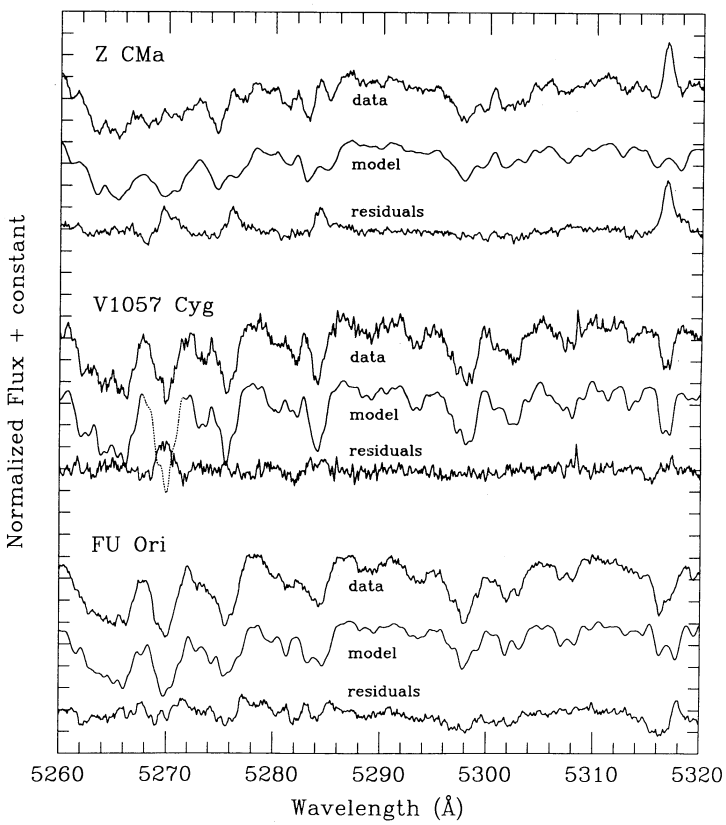

FIG. 3.—*Top to bottom*: the observed, synthesized, and residual spectra for Z CMa, V1057 Cyg, and FU Ori for several wavelength ranges. In general, the model fits well. Residual features appear in the same lines in all three objects, except that FU Ori has some the other two do not. Residual profiles vary among the objects, possibly due in part to geometric effects. The obvious features in common all are found in the list of emission lines in the "high-state" spectrum of Z CMa (Hessman et al. 1991). Tick mark spacing is 0.1 times the continuum level. Dotted portions are for clarity only.

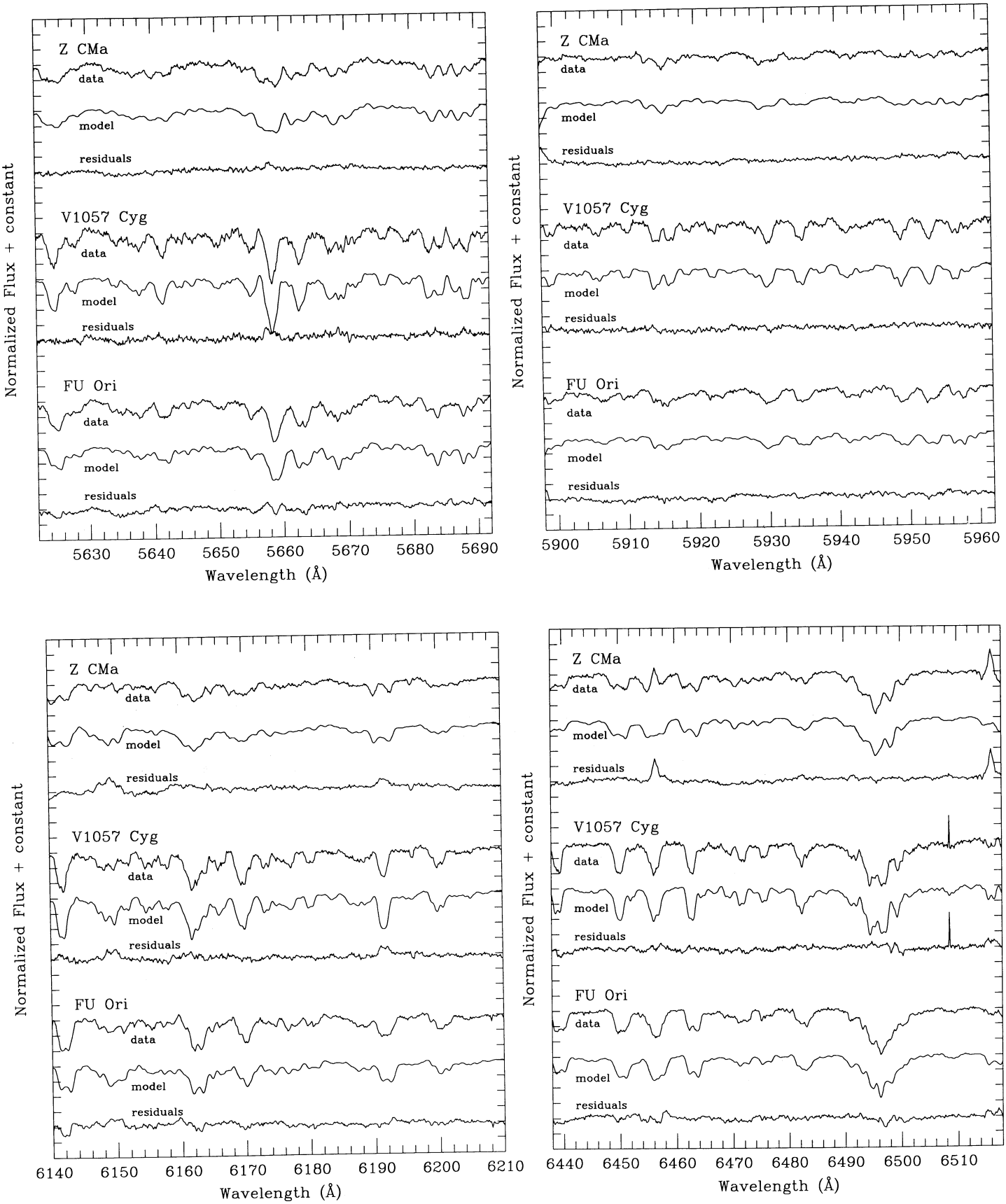

FIG. 3—*Continued*

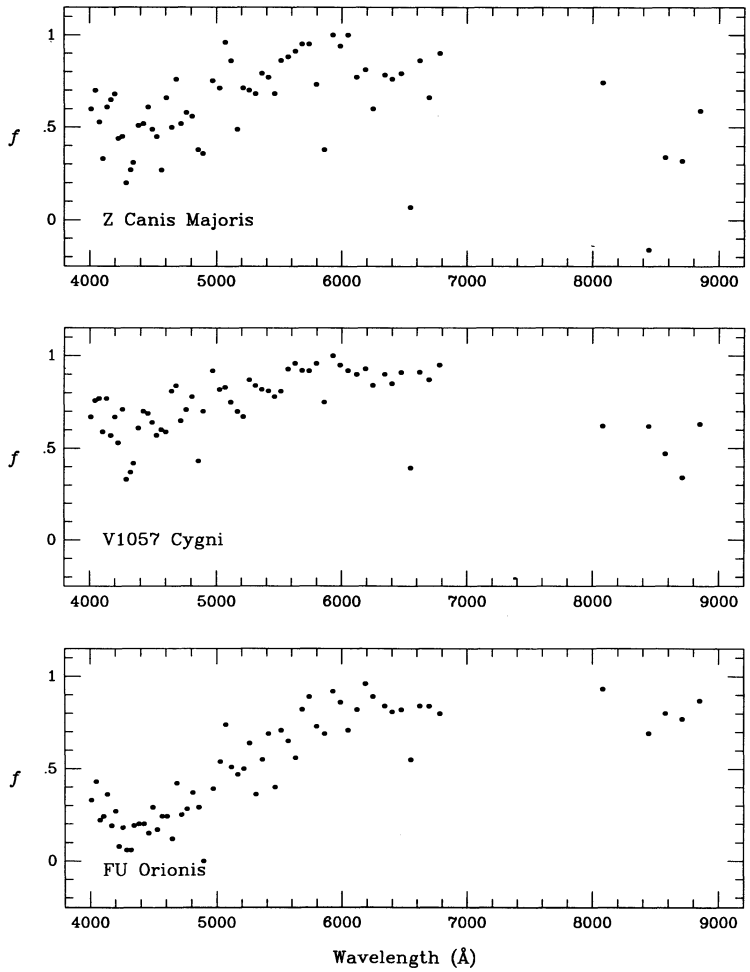

FIG. 4.—The goodness of fit (see text) is plotted against wavelength. Each point is taken from a single echelle order. Wavelength bins are contiguous where possible, and regions of heavy telluric contamination are not included. A value of 1 indicates a "perfect fit," to within the limits of the threshold value chosen and number of consecutive pixels required. Residual features are stronger and more common at short wavelengths, leading to the low values of f there. Points representing regions containing the Na I D and Hα lines are noticeably lower than neighboring points because such broad nondisk features "fool" the goodness of fit algorithm. The upturn at the short wavelength end is not real but reveals that our goodness of fit scheme should not be trusted when the signal-to-noise ratio of the spectra is low.

disks, then we may search the residual spectra for signatures of additional physical phenomena, e.g., winds. If such signatures can be identified, we will have learned more about the nature of FU Ori objects and explained some of the apparent shortcomings of the model.

Despite the great success of the accretion disk model, we feel it is essential to explore its appropriateness further. In particular, there is no reason to expect that observed disk spectra should be well matched in all details by weighted ensembles of normal stellar photospheric spectra. Our data lend themselves to two simple tests that might reveal subtle differences between supergiant and disk atmospheres. First, we search our object and synthetic spectra for features that are sensitive to gravity, providing an indication of the average local g in the inner regions of a disk. Second, we search for temperature-sensitive features, which might provide an indication of the vertical (perpendicular to the disk midplane) temperature structure of the disk. Both tests will assist in judging whether it is appropriate to compare FU Ori object spectra with models constructed from supergiant spectra. Provided these tests do not lead us to question the use of supergiants to model FU Ori object spectra, we may proceed to search the residual spectra for signatures of activity or structures other than the disks.

5.1. *Identification of Residual Features*

The first step in the analysis of the residual spectra is simply to compile a list of the residual features for each program object. This is accomplished as part of the goodness of fit procedure described in § 4. We plot each of the strong ($W_\lambda \geq$ 125 mÅ for Z CMa and V1057 Cyg, $W_\lambda \geq 200$ mÅ for FU Ori) residual features for which we are confident of identification (of the dominant contributor) on a common velocity scale in Figures 5, 6, and 7. Hundreds of weaker features are also present; details are available on request.

5.2. *Gravity Sensitivity*

Most FU Ori object spectral type determinations that include luminosity class assign class I or II to them (see Herbig 1977). There is some suggestion, however, that FU Ori objects (FU Ori in particular) may be characterized by gravity *lower*

than that of supergiants (HK1, KHH). The structure of residual features that are particularly sensitive to gravity may enable us to determine better the appropriate luminosity class for FU Ori objects. If an FU Ori *disk* has gravity *lower* than that of the standards used for spectrum synthesis, its absorption lines will generally be deeper than corresponding synthetic lines. In the absence of significant nondisk contributions, we therefore expect to find *absorption* features in the residual spectrum. Residual features due to line strength mismatch alone should have doubled profiles.

We determine which spectral lines are particularly sensitive to gravity by comparing a supergiant and a giant of roughly the same temperature (to avoid temperature sensitive lines). Standards employed were observed during the 1988 November observing runs unless noted otherwise. Of the standard star spectra available to us, the following were the best pairs for near equivalence in temperature and consistency among the three wavelength regions observed: ϵ Gem (G8 Ib) and β Gem (K0 III) for the 4000–4920 Å region, SAO 22820 (K0 Ib) and 46 LMi (K0 III; 1988 January) for the 5125–6830 Å region, and ϵ Gem (G8 Ib) and η Cyg (K0 III, 1989 December) for the 8030–9000 Å region. Note that the 4940–5125 Å range is not represented because we have no appropriate class III standard at those wavelengths.

We measure the equivalent widths of a sample of lines in each standard. The sample we have chosen includes all the strong residual features for which we are confident of identifications (i.e., those that appear in Figs. 5, 6, and 7), and the lines represented in our line width versus wavelength and line width versus excitation potential plots, chosen because they are rela-

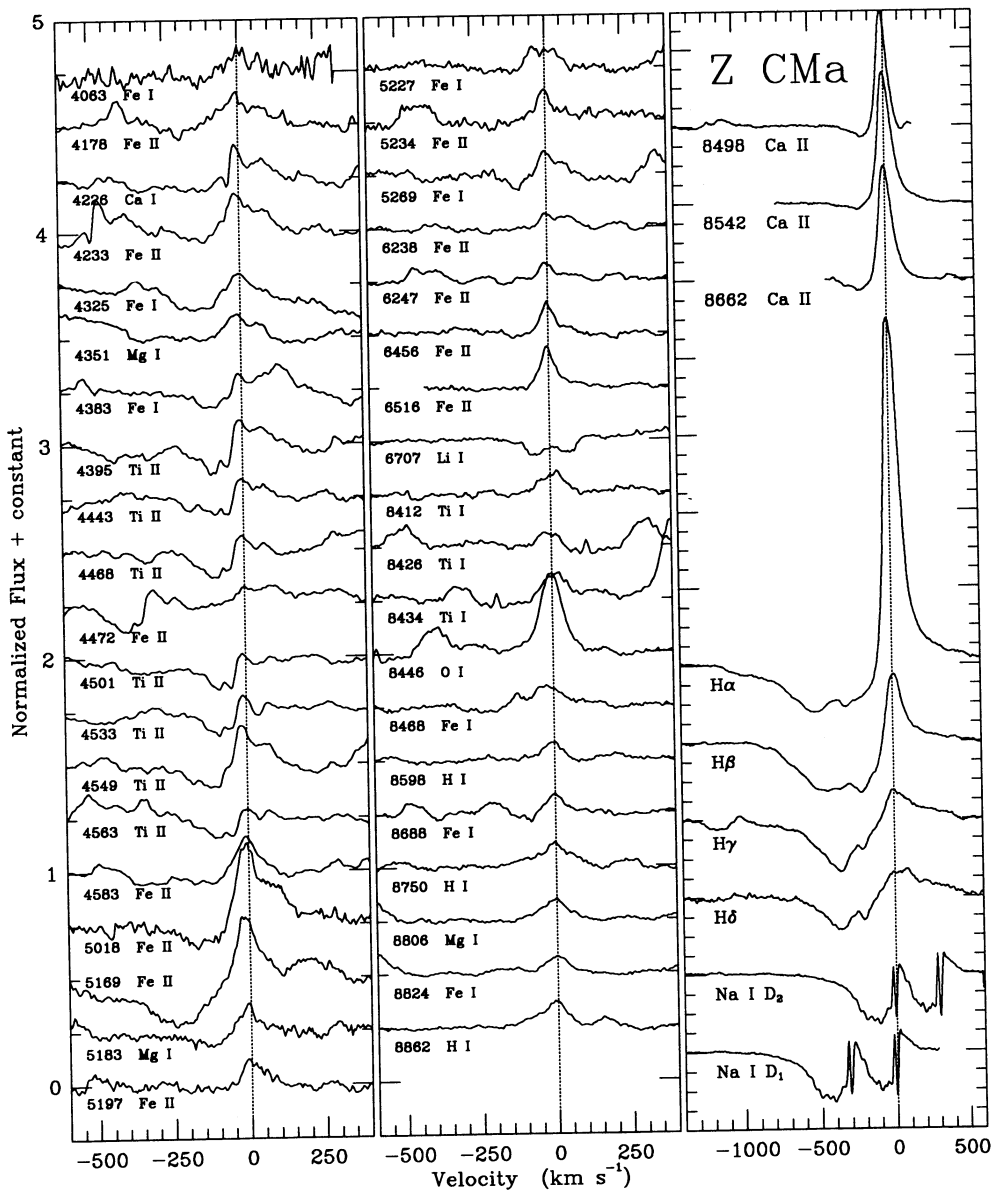

FIG. 5.—The identified strong ($W_\lambda \geq 125$ mÅ) residual features for Z CMa are plotted here on a velocity scale. Note that most features shortward of 7000 Å have P Cygni structure, while those at longer wavelengths are emission features. We believe physical conditions which violate the assumptions of the simple disk model are responsible for the long wavelength emission residuals.

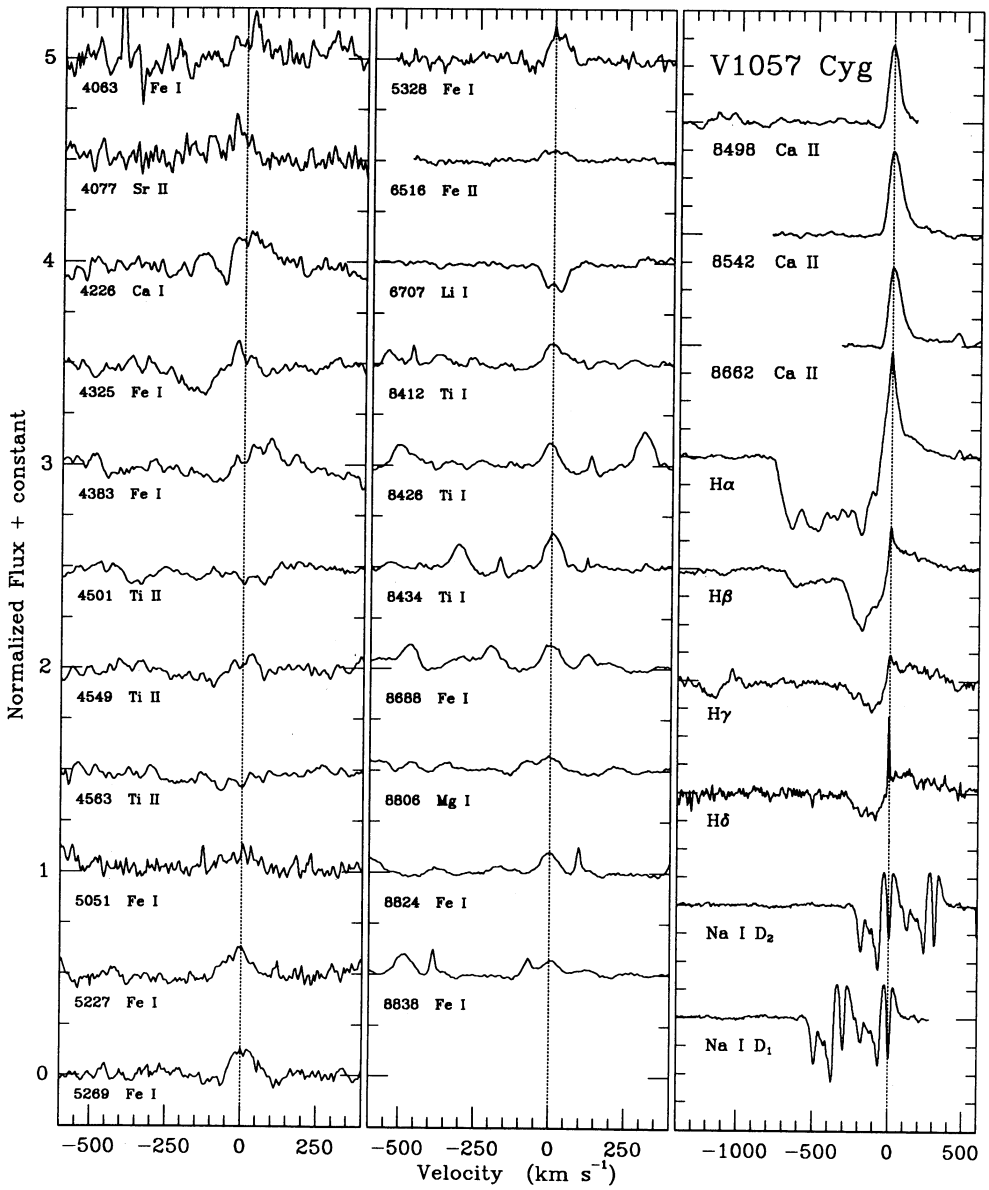

FIG. 6.—Same as Fig. 5, for V1057 Cyg

tively unblended.[7] A particularly gravity sensitive spectral line is defined arbitrarily as one for which the ratio of equivalent widths in the supergiant and the giant is greater than 3.0. We find a total of 17 such lines in the sample of 180. The ratio for the majority of lines in the sample ranges from 1.5 to 2.5. In general, lines from ionized species tend to have a larger equivalent width ratio than lines from neutral species, as expected. There are no lines in the sample that are significantly stronger in the giant than in the supergiant. We have not carried out this analysis for the complete residual feature lists because we believe uncertainties in, for example, continuum normalization make such identifications less useful when weaker residual features are considered.

Very few of the lines most sensitive to gravity appear in the lists of strong residual features. The λ6707 Li I line, strong in the spectra of FU Ori objects (and in the residual spectra) because of their youth, is noted as being particularly sensitive to gravity in our analysis. This is due to an anomalously strong Li I line in the K0 Ib standard. No lines in Figure 6 (V1057 Cyg) are especially gravity sensitive as defined here. In Figure 5 (Z CMa) seven lines are gravity sensitive: two Ti II and five Fe II lines. Both Ti II lines have obvious P Cygni structure. The Fe II lines are emission only, at the systemic velocity, but are narrower than typical photospheric absorption lines. We believe they are weak, "posteruption" state versions of the strong emission lines seen during a small (0.7 mag) outburst in 1987 February (Hessman et al. 1991). Only one P Cygni feature in Figure 7 (FU Ori) is identified as particularly gravity sensi-

[7] There is no overlap in these groups for FU Ori, i.e., the lines used for line width vs. wavelength and line width vs. excitation potential do not have strong unblended residuals; there are only (the same) three lines common to both lists for Z CMa and V1057 Cyg. This confirms the utility of those lines for model prediction tests in addition to the criteria given in § 3.

tive. If our standard stars are of inapproprate gravity and the disk dominates the spectrum, we expect residual gravity sensitive features to have profiles similar to those of disk absorption lines. Thus we find no evidence from this analysis that the surface gravity of our program objects differs radically from these stars we used for spectrum synthesis.

The relative proportions of absorption and emission residuals give us additional information. Since most absorption lines are stronger in lower gravity stars, an absorption residual would suggest that the object has lower surface gravity than the synthetic spectrum. Shortward of 6000 Å in V1057 Cyg and Z CMa there is a slight preference for emission residuals. Longward of 6000 Å, non–P Cygni residuals are almost exclusively emission features. While this suggests these objects possess gravity higher than that of supergiants, especially at longer wavelengths, it may be that physical conditions which violate the assumptions of the simple disk model are responsible for the presence of residual emission features.

The behavior in FU Ori is different. Of its 57 strong ($W_\lambda \geq$ 200 mÅ), non–P Cygni residuals, 56 are absorption features. Roughly 67% of all FU Ori's residual features are in absorption (as opposed to 50% for Z CMa and V1057 Cyg). While this suggests gravity lower than that of supergiants, as suggested by HK1, it is not conclusive; strong absorption in the FU Ori wind may be responsible.

5.3. *Temperature Sensitivity*

Although we have used our goodness of fit test to determine the best T_{max} values to use in synthetic disk calculations, we can test our results further by analysis similar to that for gravity sensitivity. With the supergiants in the previous section, we used β Aqr (G0 Ib), SAO 22740 (G2 Ib), and μ Per (G0 Ib) for

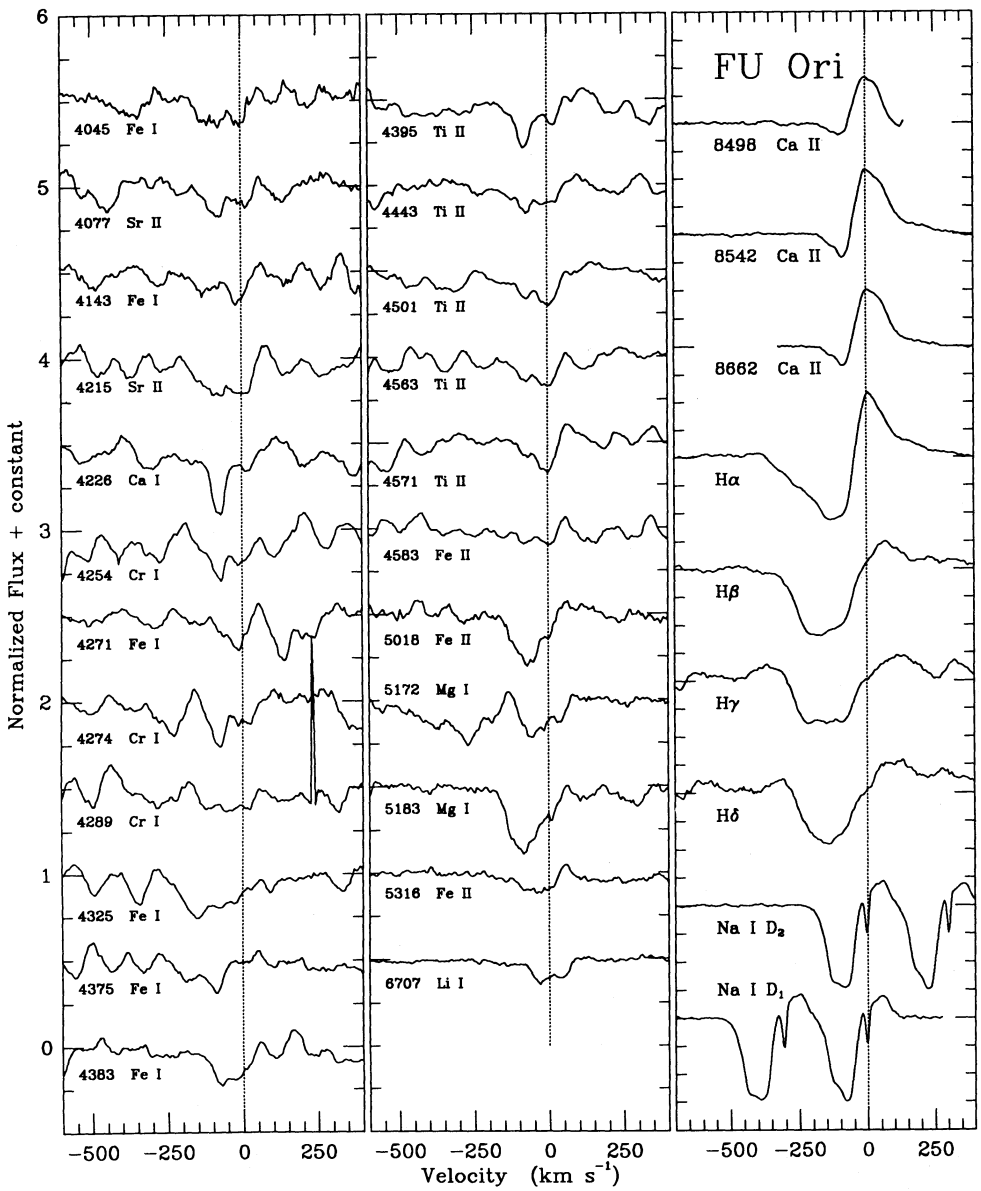

FIG. 7.—Same as Fig. 5, for FU Ori. The equivalent width cutoff is 200 mÅ.

the 3985–4920 Å, 4940–6830 Å, and 8030–9000 Å regions, respectively. To flag an especially temperature sensitive line, we require an equivalent width ratio greater than 2.75. We find 17 such lines in the sample of 180, while most lines have a ratio between 1 and 2. We remove the λ6707 Li I line from consideration for the same reason as above.

Only two of the 17 most temperature sensitive lines appear in the strong residual feature figures. The λ4226 Ca I line appears as a P Cygni residual in V1057 Cyg and Z CMa, and the λ6516 Fe II line is in emission in the V1057 Cyg residual spectrum. So we find no significant evidence that we have made an error in disk temperature scale normalization for any of our program objects.

5.4. *Description of Residual Features*

All the analysis of the residual spectra to this point has led to the conclusion that the features present in the residual spectra of our program objects are intrinsic to those systems, and not due to errors in disk model parameters or to sensitivity to physical conditions in the disks. The presence of obvious wind signatures in the Na I D, Balmer, and Ca II infrared triplet, and the P Cygni structure of many of the residual features leads us to interpret the residual features as additional signatures of the powerful FU Ori winds. We wish to know whether they hold any information that can be used to better determine the properties of those winds. Here we offer descriptions of trends seen in the residual features in each object.

5.4.1. *Z Canis Majoris*

The high signal-to-noise ratio in our Z CMa spectra and relative strength of residual features provide a good opportunity to characterize the residual spectrum of Z CMa. At short wavelengths there are many P Cygni profiles with doubled emission, with peaks at about -5 and $+65$ km s^{-1}, changing to pure emission features at ~ 0 km s^{-1} at longer wavelengths.

In Figure 8 we show the average of all the unblended (as judged by visual inspection and comparison with line lists) residual features for two Fe I multiplets. The upper profile (five lines from Fe I multiplet 43, lines near 4100 Å) shows a distinct pair of emission peaks, at -5 and $+64$ km s^{-1}. The blue absorption extends to -200 km s^{-1}, and the red emission wing to $+110$ km s^{-1}. In the middle profile (nine lines from Fe I multiplet 15, lines near 5400 Å) the distinct red emission has become a less conspicuous "shoulder" on the main 0 km s^{-1} peak. The blue absorption extends to -170 km s^{-1}, and the red wing to $+90$ km s^{-1}. Many of the other residual features follow the same basic pattern.

The bottom profile in Figure 8 is the average of the Ti II lines in Figure 5 (seven relatively unblended lines from several multiplets, in the 4500 Å region). Here we see the doublet emission, but additional structure is present within the blue absorption. Several more blended Ti II lines (e.g., 4294 Å, 4300 Å, 4571 Å) apparently share this structure. It is structure such as this that we believe may ultimately enable us to determine the structure of the Z CMa wind.

In the Na I D and Balmer lines, the model subtraction has enabled the P Cygni appearance of the lines. We note the very distinct components present in the Na I D lines (the zero velocity features are probably of interstellar origin), and the decrease in maximum wind speed through the Balmer series, probably a signature of wind acceleration (to at least 1200 km s^{-1}, the extent of the blue wing of Hα). We note however that model subtraction of these lines may not be appropriate, as the Na I D wings are sensitive to photospheric conditions and Hα profiles may have a strong chromospheric component (Croswell et al. 1987).

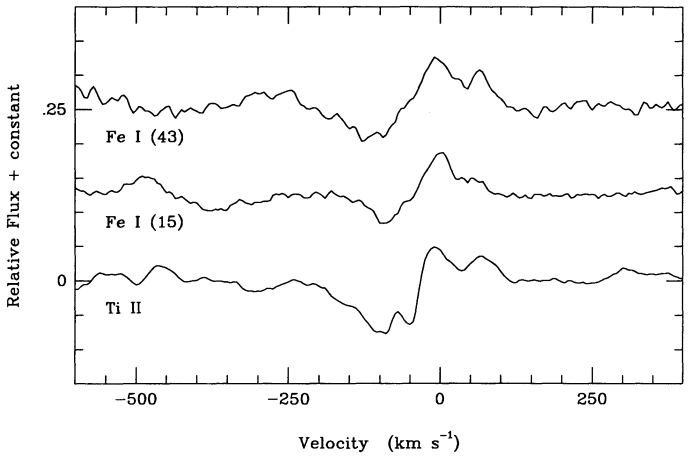

FIG. 8.—Average profiles for relatively unblended residual features. Fe I multiplet 43 lines all have wavelengths near 4100 Å and LEP ~1.6 eV, while multiplet 15 lines are in the 5200–5500 Å region and have LEP ~0.95 eV. The Ti II lines included are from several multiplets, range in wavelength from 4395 to 4563 Å, and have LEP ~1.2 to ~1.6 eV. The variation of profiles with wavelength, excitation, etc., may enable us to determine the structure of Z CMa's wind.

5.4.2. *V1057 Cygni*

As noted above, most of the far-red (8030–8900 Å) residual features in V1057 Cyg are emission features centered at the systemic velocity, suggesting a departure from simple disk model assumptions in the outer disk. We discuss the cause for this departure below and ignore such features in the present discussion. At the shortest wavelengths, meaningful structure is apparent in the strongest residuals. Many of them (e.g., the first eight in Fig. 6) have two distinct peaks at about $+30$ and -30 km s^{-1}, and many have blue absorption extending to ~ -200 km s^{-1}. The double peaked structure and blue absorption become less apparent toward longer wavelengths. The behavior of the Balmer lines is similar to that in Z CMa in indicating the acceleration of the wind to very high velocity ($\gtrsim 800$ km s^{-1}).

5.4.3. *FU Orionis*

Because of the uncertainty in the origin of the residuals in FU Ori (probably wind, evidenced by a ~5 km s^{-1} blueshift of residual features found in cross-correlation studies, or possible inappropriate gravity in the model spectra), and because of the severe blending apparent even in the features we have tentatively identified (see Fig. 8), we are not in a position to discuss trends in residual line profiles at this time. However, we do note similarity to Z CMa and V1057 Cyg in that the frequency or residual features decreases with wavelength, and many of FU Ori's stronger residual features correspond to strong residuals in the other two objects. This likeness, together with evidence presented in §§ 3 and 4, suggests that similar activity is occurring in all three systems.

Herbig (1966) identified a number of "shell" absorption features, displaced ~80 km s^{-1} blueward, in spectra of FU Ori. Several of these are apparent in the residual spectrum: 4077 Å, 4226 Å, 4246 Å, 4254 Å, 4274 Å, 4395 Å, 5018 Å, and 5183 Å.

Most of the features in the first two panels of Figure 8 also have an emission peak at $\sim +65$ km s^{-1}.

5.5. *Constraint of Wind Properties*

We have shown that the accretion disk model provides a good representation of high-resolution optical spectra of the FU Ori objects, and that residual features in difference spectra are real and intrinsic to the FU Ori systems. Because most of the strongest residual features have P Cygni structure, and because these objects are known to drive powerful winds (evident from their Hα and Na I D lines), it is natural to interpret the residual features as additional signatures of the FU Ori object winds. Detailed analysis of those features may provide clues to the origin and nature of the winds.

Such analysis, and theoretical calculations of wind profiles, are beyond the scope of this paper and will be pursued in future work. However, it is clear from profile shapes and wavelength dependence that spherical geometry is ruled out. We believe efforts which recognize the presence of a rapidly rotating disks in these systems, and the likelihood that winds may arise directly from those disks, will be the most fruitful.

6. CONCLUSIONS

We have used high-resolution, high signal-to-noise ratio optical spectra to investigate the accretion disk hypothesis to the FU Ori objects. That hypothesis suggests that in outburst, FU Ori objects are self-luminous accretion disks, whose light dominates at optical and near-infrared wavelengths. Such a disk ideally has a characteristic radial temperature gradient, $T(R) \propto R^{-3/4}$ (for $R \gg R_*$), and a Keplerian rotation curve. If each point of such a disk radiates as a star of type appropriate to the local temperature, the net line spectrum should contain signatures of this temperature and velocity structure.

We have investigated predicted correlations between line width and both wavelength and lower excitation potential in synthetic and observed FU Ori object spectra. Strong evidence has been found for line width versus wavelength correlation in good agreement with model prediction for Z CMa and V1057 Cyg, but not for FU Ori itself. We emphasize that line width varies *continuously* with wavelength at optical wavelengths in the former two objects. In the case of FU Ori, we argue that a combination of strong wind components to spectral lines, and surface gravity possibly being lower than that of supergiants (used in calculation of synthetic spectra), conceals the underlying line width versus wavelength relationship.

We find marginal correlation between line width and lower excitation potential in all three program objects. In the case of V1057 Cyg, we confirm earlier detection of this effect. In each case we find reasonable agreement with model prediction. Apparently line width variation with excitation potential is a subtle effect and is less useful than the variation of line width with wavelength as a diagnostic of differential rotation.

Satisfied that the accretion disk model is an adequate first-order approximation to the FU Ori object spectra, we subtracted our best synthetic (model) disk spectra from the observed spectra to produce residual spectra. A goodness of fit quantity was defined (essentially the number of object line profiles that are fitted well by the synthetic disk spectral lines) to determine quantitatively how well a given model reproduces an FU Ori object spectrum. We defined the best model for each object as that which maximizes the goodness of fit. For those best models, $\gtrsim 85\%$ of spectral features are well fitted (to ~ 10 mÅ accuracy) in regions of the spectrum not strongly affected by nondisk components (~ 5500–6800 Å).

Based on their structure, as well as the goodness of fit testing, we verify that residual features present are intrinsic to the FU Ori systems, and not due to errors in model parameters or peculiar sensitivity to physical conditions. These residual features are interpreted as signatures of the powerful winds driven by FU Ori objects.

We argue that complex residual line structure, evident most clearly in Z CMa, is real and probably does not arise in a simple radial outflow arising from a central star. We suggest that FU Ori winds are ejected from the rapidly rotating inner disk regions, and probably carry large amounts of angular momentum away from these systems.

Several interesting avenues for future work are suggested. Changes in FU Ori object spectra with time will be important in further confirmation of the accretion disk hypothesis. In particular, the model predicts that absorption line widths should increase as a disk cools. We have observed this effect in our spectra of V1057 Cyg (1986 October through 1989 December). Based on just four lines, we have also noticed an increase in Z CMa's line widths, from 1983 December to 1988 November. From our 1986 December to 1989 November spectra of FU Ori, no such line width increase is seen. We will report further in a subsequent paper.

We have pointed out that our modeling could be improved by more careful selection of standard stars and by more complete spectral type coverage. Improved modeling and improved signal-to-noise ratio data, especially of V1057 Cyg, will be important for better determination of the residual (wind) spectra of the FU Ori objects. Such study of other members of the class will also be instructive. Once better residual spectra are available, an in-depoth study of the residual features, including modeling of residual spectra, will be crucial in determining the location and mechanism of wind production and the physical processes that influence those winds after initial acceleration.

Other issues include deviations of real physical conditions from model assumptions. In particular, the problem of possible disk flaring and its effect on the disk's line spectrum, should be investigated. Whether the radial temperature distribution of a classical accretion disk (LBP) and Keplerian velocity distribution are appropriate are questions deserving attention.

Beyond testing various models for FU Ori objects and their outbursts, effort should continue to be made to detect more such objects. Discovery of all FU Ori objects will help determine the frequency of FU eruptions, and their overall importance in building up the central stars involved. Detailed observation of FU Ori outbursts as they occur will be invaluable for constraining models for the outbursts of these fascinating objects.

We gratefully acknowledge the Kitt Peak staff for their assistance during our observing runs, and Rob Hewett for data handling and help with aspects of disk modeling. A. D. W., S. E. S., and S. E. were supported by grants from the NASA Planetary Program, the NASA Astrophysics Data Program, and the National Science Foundation. This research was supported in part by the Scholarly Studies program of the Smithsonian Institution.

REFERENCES

Bastian, U., & Mundt, R. 1985, A&A, 144, 57
Carr, J., Harvey, P. M., & Lester, D. F. 1987, ApJ, 321, L71
Croswell, K., Hartmann, L., & Avrett, E. H. 1987, ApJ, 312, 227
Eislöffel, J., Hessman, F. V., & Mundt, R. 1990, A&A, 232, 70
Elias, J. 1978, ApJ, 223, 859
Graham, J. A., & Frogel, J. A. 1985, ApJ, 289, 331
Hartmann, L., & Kenyon, S. J. 1985, ApJ, 299, 462 (HK1)
———. 1987a, ApJ, 312, 243 (HK2)
———. 1987b, ApJ, 322, 393 (HK3)
Hartmann, L., Kenyon, S. J., Hewett, R., Edwards, S., Strom, K. M., Strom, S. E., & Stauffer, J. R. 1989, ApJ, 338, 1001
Herbig, G. H. 1966, Vistas Astron., 8, 109
———. 1977, ApJ, 223, 213
———. 1989, in ESO Workshop on Low Mass Star Formation and Pre–Main-Sequence Objects, ed. B. Reipurth (Garching: ESO), 233
Hessman, F. V., Eislöffel, J., Mundt, R., Hartmann, L. W., Herbst, W., & Krautter, J. 1991, ApJ, 370, 384
Kenyon, S., & Hartmann, L. 1988, in Pulsation and Mass Loss in Stars, ed. R. Stalio & L. A. Willson (Dordrecht: Kluwer), 133
Kenyon, S. J., Hartmann, L., & Hewett, R. 1988, ApJ, 325, 231 (KHH)
Koresco, C. D., Beckwith, S. V. W., Ghez, A. M., Matthews, K., & Neugebauer, G. 1991, AJ, 102, 2073
Levreault, R. M. 1983, ApJ, 265, 855
Lynden-Bell, D., & Pringle, J. E. 1974, MNRAS, 168, 603 (LBP)
Moore, C. E. 1959, A Multiplet Table of Astrophysical Interest (NBS TN 36, PB 151395) (Springfield, VA: Department of Commerce, Clearing House for Federal and Scientific Information)
Moore, C. E., Minnaert, M. G. J., & Houtgast, J. 1966, The Solar Spectrum 2935 Å to 8770 Å (NBS Monog. 61) (Washington, DC: Department of Commerce)
Mundt, R., Stocke, J., Strom, S. E., Strom, K. M., & Anderson, E. R. 1985, ApJ, 297, L41
Reipurth, B. 1985a, A&A, 143, 435
———. 1985b, in Proc. ESO-IRAM-Onsala Workshop on (Sub)Millimeter Astronomy, ed. P. A. Shaver & K. Kjär (Garching: ESO), 458
Staude, H. J., & Neckel, Th. 1991, A&A, in press
Swenson, J. W., Benedict, W. S., DelBouille, L., & Roland, G. 1970, The Solar Spectrum from λ7498 to λ12016 (Liège: Société Royale des Sciences de Liège)
Welty, A. D., Strom, S. E., Strom, K. M., Hartmann, L. W., Kenyon, S. J., Grasdalen, G. L., & Stauffer, J. R. 1990, ApJ, 349, 328